Applied Environmental Research (2026) 48(3), 021
https://doi.org/10.35762/AER.2026021

Applied Environmental Research
- RESEARCH FOR SUSTAINABLE PLANET -

Research Article

Ammonium Adsorption from Aqueous Solutions Using $MnFe_2O_4$-Functionalized Coffee Husk Biochar Nanocomposites: An Evaluation of HNO_3 and NaOH Activation

Thuy-Tien Do[1], Huu-Tap Van[2,*], Thi-Minh-Thu Nguyen[3]

[1] *Department of Chemistry, Hanoi Pedagogical University 2, 32 Nguyen Van Linh, Xuan Hoa, Phy Tho, Vietnam*
[2] *Center for Advanced Technology Development, Thai Nguyen University, Bac Son road, Phan Dinh Phung ward, Thai Nguyen, Vietnam*
[3] *Environment Agency, Ministry of Agriculture and Environment, No.10 Ton That Thuyet street, Hanoi, Vietnam*

*Corresponding Email: vanhuutap@tnu.edu.vn

Abstract

This research investigated the development of $MnFe_2O_4$-based composite adsorbents (MFO@CFA and MFO@CFB) by activating coffee husk-derived biochar with HNO_3 and NaOH, followed by synthesis through coprecipitation and hydrothermal techniques. The structural and chemical properties of the nanocomposites were characterized by scanning electron microscopy (SEM) and Fourier transform infrared (FTIR) spectroscopy. Batch adsorption experiments were used to assess ammonium removal efficiency across a range of conditions: solution pH (3–8), contact time (5–120 min), adsorbent dosage (0.2–3 g L^{-1}), and initial ammonium concentration (10–60 mg L^{-1}). The findings indicated that compared with MFO@CFB, which was synthesized from NaOH-activated biochar, MFO@CFA, derived from HNO_3-activated biochar, presented enhanced surface functionality and a superior adsorption capacity. Langmuir isotherm analysis revealed maximum adsorption capacities of 55.25 mg g^{-1} for MFO@CFA and 28.73 mg g^{-1} for MFO@CFB, highlighting the potential of MFO@CFA as an effective adsorbent for ammonium remediation in wastewater treatment. Reusability tests over five adsorption–desorption cycles revealed that MFO@CFB and MFO@CFA retained more than 50% of their initial NH_4^+ adsorption capacity after regeneration, which was supported by alkaline desorption and stable $MnFe_2O_4$-enabled magnetic separation.

ARTICLE HISTORY

Received: 4 Sep. 2025
Revised: 18 Dec. 2025
Accepted: 16 Feb. 2026
Published: 25 Feb. 2026

KEYWORDS

Ammonium adsorption;
$MnFe_2O_4$ nanocomposite;
Coffee husk biochar;
Wastewater treatment;
Adsorption isotherms

Introduction

The escalation of industrialization, urbanization, and population growth has intensified the contamination of natural water resources, posing significant threats to environmental sustainability. Among the prevalent contaminants, ammonium ions (NH_4^+) are a major concern because of their substantial contribution to the degradation of surface and groundwater quality (Puari et al., 2023). Originating primarily from agricultural runoff, municipal wastewater, and industrial effluents (Puari et al., 2023; Yang et al., 2023), ammonium promotes eutrophication, leading to hypoxic conditions and toxicity to aquatic biota (Phuong et al., 2021). Consequently, the development of efficient and sustainable technologies for ammonium remediation has become a critical research imperative in environmental engineering.

The existing ammonium removal techniques include adsorption, air stripping, chemical precipitation, electrochemical oxidation, and biological denitrification. However, air stripping is energy intensive, and chemical precipitation often generates secondary pollutants, limiting their practical applicability. Adsorption has emerged as a preferred method because of its operational simplicity, cost-effectiveness, and minimal environmental footprint. Biochar, a carbon-rich material derived from biomass pyrolysis, has gained significant attention for

its tunable surface chemistry and sustainability as an adsorbent (Vu et al., 2017). Recent studies have explored strategies to increase the ammonium adsorption capacity of biochar, including surface functionalization with acids, alkalis, or oxidants and impregnation with metal or metal oxide nanoparticles (Han et al., 2021; Nguyen et al., 2021; Yang et al., 2023). $MnFe_2O_4$-based materials have been widely applied as adsorbents for removing heavy metals, organic dyes, pesticides, and other contaminants from aqueous solutions (Asghar et al., 2020; Huong et al., 2018; Liao et al., 2020; Taguba et al., 2021). Notably, compared with standalone materials, $MnFe_2O_4$/carbon nanocomposites synergistically combine the adsorption properties of activated carbon with the magnetic and catalytic attributes of $MnFe_2O_4$, resulting in superior adsorption performance (Tuyen et al., 2020). The oxygen-containing functional groups on activated carbon, such as carboxyl (-COOH), hydroxyl (-OH), and alkoxy (-C-O) groups, significantly enhance adsorptive interactions (Wan et al., 2014).

Dak Lak Province has the largest coffee-growing area in Vietnam, with coffee production reaching approximately 535,000 tons in 2024. As dried coffee cherry husks account for approximately 60–65% of the harvested cherries, the province generates nearly 320,000 tons of this agricultural residue annually. Compared with other agricultural residues, this waste decomposes relatively slowly, leading to potential environmental pollution if not properly managed. In Vietnam, this byproduct has been valorized for various applications, such as soil conditions, animal feed production, and fertilizer production, particularly for biochar production.

Despite these advancements, the application of $MnFe_2O_4$/biochar nanocomposites derived from agricultural residues, such as coffee husks, for ammonium remediation remains largely underexplored. Prior research has focused primarily on individual $MnFe_2O_4$ or unmodified biochar systems, with few studies addressing the optimization of nanocomposite adsorbents for ammonium removal. Kizito et al. (2015) investigated the adsorption capabilities of wood and rice husk biochar, specifically in terms of ammonium removal from anaerobic pig manure sludge. Their findings revealed an adsorption efficiency of up to 60%. In 2018, Khalil et al. (2018) investigated the ammonium adsorption capacity of biochar produced from rice straw modified with 0.1 M NaOH (denoted as RSII). The results showed that RSII achieved 43% NH_4^+ removal efficiency and a maximum adsorption capacity of 2.9 mg g^{-1} at an initial ammonium concentration of 12 mg L^{-1} and pH 7.5. Adsorption equilibrium was reached after 90 minutes, with an optimal pH range of 7–8. Furthermore, assessments by Han et al. (2021) demonstrated that the use of low-cost materials is an effective and promising approach for environmental remediation. Notably, bentonite exhibited substantial ammonium adsorption performance, with a maximum NH_4^+ adsorption capacity of 19.01 mg g^{-1} and a removal efficiency of 53.4% at pH 7. The treatment efficiency increased to 81.2% when the adsorbent dosage was increased to 40 g L^{-1}. Vu et al. (2023) explored the potential of using coffee husks for biochar production and subsequently assessed their effectiveness in removing ammonium from wastewater. Their results indicated a significant adsorption capacity of 2.8 mg g^{-1} after 6 hours. Further investigations into the use of agricultural residues have revealed that biochars produced from these materials can effectively remove ammonium from water. Liu et al. (2016) demonstrated that alkali-modified biochars derived from agricultural residues exhibited enhanced ammonium adsorption capacities, indicating the potential to optimize biochar properties through chemical modification. Lin et al. (2024) evaluated the NH_4^+ adsorption performance of biochar produced from extracted coffee grounds and reported that, within an initial pH range of 4–8, an equilibrium contact time of 90 min, an optimal solid–liquid ratio of 10 g L^{-1} and an initial NH_4^+ concentration below 25 mg L^{-1}, the material achieved a removal efficiency of 77.6% and a maximum adsorption capacity (q_{max}) of 14.48 mg g^{-1}.

Although $MnFe_2O_4$-doped carbon nanocomposites have shown excellent performance in heavy metal and dye removal, their application for ammonium (NH_4^+) adsorption is critically constrained by four interconnected limitations that have not been adequately addressed. First, most composites are synthesized via unmodified or weakly activated biochar, resulting in insufficient negatively charged surface sites (e.g., –COOH/–COO^-), which are indispensable for strong electrostatic capture of cationic NH_4^+. Second, limited pore development and a low specific surface area (<20 m^2 g^{-1}) severely restrict NH_4^+ diffusion and site accessibility, capping reported capacities below 20 mg g^{-1}. Third, the high point of zero charge (pH_{PZC} > 6), which is typical of NaOH-only activated supports, narrows the effective pH operating window, rendering these materials ineffective in mildly acidic wastewater (pH 5–6). Fourth, and most critically, no prior study has systematically compared acid (HNO_3) versus alkali (NaOH) activation strategies to engineer the $MnFe_2O_4$–biochar interface for enhanced NH_4^+ binding affinity, capacity and pH resilience. These unresolved deficiencies constitute a major technological and mechanistic gap in the development of high-performance, magnetic, biochar-based adsorbents for sustainable ammonium remediation from aqueous environments.

The novelty of this study lies in the development of a $MnFe_2O_4$/biochar nanocomposite synthesized from coffee husk-derived biochar chemically modified with HNO_3 and NaOH to enhance surface functionality. This approach not only valorizes an abundant agro-

industrial byproduct but also introduces a sustainable, cost-effective adsorbent with enhanced ammonium adsorption capacity. The nanocomposites were prepared via coprecipitation and hydrothermal synthesis, and their performance was systematically evaluated by analyzing key parameters, including the solution pH, contact time, adsorbent dosage, and initial ammonium concentration. By elucidating the synergistic interactions between $MnFe_2O_4$ and modified biochar, this research addresses a critical knowledge gap, offering a high-performance, eco-friendly solution for ammonium removal in wastewater treatment and advancing the field of environmental remediation technologies.

Materials and methods

1) Chemicals and instrumentation

The synthesis and evaluation of the $MnFe_2O_4$/biochar nanocomposites utilized the following analytical-grade reagents: manganese(II) chloride tetrahydrate ($MnCl_2 \cdot 4H_2O$, 99%, Merck, Germany), iron(III) chloride hexahydrate ($FeCl_3 \cdot 6H_2O$, 99%, Merck, Germany), nitric acid (HNO_3, 63%), sodium hydroxide (NaOH, 96%), ethanol (Aladdin, China), potassium sodium tartrate tetrahydrate ($KNaC_4H_4O_6 \cdot 4H_2O$, 50%), ammonium chloride (NH_4Cl, Merck), Nessler's reagent (Merck), and deionized water. Coffee husk, an agricultural byproduct, was sourced locally and used as the precursor for biochar production.

The experimental setup included the following instruments: a UV–Vis spectrophotometer (Model 730, Japan) for ammonium concentration analysis, an IKA horizontal shaker for adsorption experiments, a HACH CDC401 handheld pH meter for pH measurements, an Ohaus drying oven (USA) for material drying, a centrifuge for phase separation, a laboratory oven for thermal treatments, and an analytical balance for precise mass measurements.

2) Synthesis of composite materials

2.1) Preparation of NaOH-activated biochar (CFB)

Coffee husks were thoroughly washed with distilled water to remove impurities, dried at 110 °C for 24 hours in a laboratory oven, and pulverized to a uniform particle size of 0.5–1.0 mm. The processed coffee husks were impregnated with a 0.3 M NaOH solution at 70 °C for 24 hours, maintaining a weight-to-volume ratio of 1:10 (10 g of coffee husk:100 mL of NaOH solution). The treated material was washed repeatedly with distilled water until the pH stabilized at 7–8 and then dried at 70 °C to a constant weight. Subsequently, 10 g of the treated coffee husks were placed in a porcelain crucible and carbonized in a furnace at 350 °C for 60 min under an argon atmosphere at a heating rate of 5 °C min^{-1}, yielding NaOH-activated biochar (CFB).

2.2) *Preparation of HNO_3-activated biochar (CFA)*

Coffee husks were washed with distilled water, dried at 110 °C for 24 hours, and pulverized to a particle size of 0.5–1.0 mm. The material was impregnated with a 3 M HNO_3 solution at 80 °C for 4 hours, with a weight-to-volume ratio of 1:10 (coffee husk:HNO_3 solution). The treated husks were washed with distilled water until the pH reached 7–8 and dried at 70 °C to a constant weight. The material was subsequently treated with a 0.25 M NaOH solution at a 1:10 weight-to-volume ratio, followed by washing with distilled water until the pH reached 7–8 and drying at 70 °C. A 10 g sample of the treated coffee husks was carbonized in a porcelain crucible at 350 °C for 60 min under an argon atmosphere at a heating rate of 5 °C min^{-1}, yielding HNO_3-activated biochar (CFA).

2.3) *Preparation of $MnFe_2O_4$ (MFO)*

$MnFe_2O_4$ nanoparticles were synthesized via co-precipitation. A 50 mL solution of $MnCl_2 \cdot 4H_2O$ (0.1 M) and a 50 mL solution of $FeCl_3 \cdot 6H_2O$ (0.2 M) were combined in distilled water (Mn^{2+}:Fe^{3+} molar ratio of 1:2) in a conical flask (Flask 1) and stirred magnetically for 90 mins. Concurrently, 65 mL of 2 M NaOH solution was prepared in a separate conical flask (Flask 2). Both solutions were heated to 80 °C in a water bath. The solution from Flask 1 was slowly added to Flask 2 under continuous stirring, and the mixture was maintained at 80 °C for an additional 90 mins. The resulting precipitate was filtered, washed with distilled water until the filtrate reached pH 7, and dried at 80 °C for 24 hours to obtain $MnFe_2O_4$ (MFO).

2.2) *Synthesis of $MnFe_2O_4$/biochar nanocomposites (MFO@CFB and MFO@CFA)*

$MnFe_2O_4$/biochar nanocomposites were prepared by combining $MnFe_2O_4$ (MFO) with either CFB or CFA at a weight ratio of 1:3 (MFO:biochar). Two composites were synthesized: MFO@CFB ($MnFe_2O_4$ with CFB) and MFO@CFA ($MnFe_2O_4$ with CFA). The mixtures were dispersed in 70 mL of double-distilled water in conical flasks and stirred magnetically for 3 hours. The suspensions were then transferred to Teflon-lined stainless-steel autoclaves and subjected to hydrothermal treatment at 200 °C for 12 hours. After cooling to ambient temperature, the products were centrifuged, washed with distilled water until the supernatant reached pH 7, and dried at 80 °C to a constant weight (Tuyen et al., 2020).

3) Characterization of materials

The surface functional groups of the $MnFe_2O_4$/biochar nanocomposites (MFO@CFB and MFO@CFA) were characterized via Fourier transform infrared (FTIR) spectroscopy on a Model 6300 spectrometer (Japan). The morphological and microstructural properties of the

materials were analyzed by scanning electron microscopy (SEM, Hitachi S-4800). The surface area (BET) of the nanocomposites was determined via a surface area analyzer (Micromeritics TriStar 3030-USA).

The point of zero charge (pH_{PZC}) of the nanocomposites was determined via a pH titration method. A 0.1 M NaCl solution was used as the electrolyte and was maintained at a constant temperature of 25 °C. Triplicate 50 mL aliquots of the NaCl solution were placed in conical flasks, and their initial pH (pH_i) was adjusted to 2, 4, 6, 8, 10, or 12 using 0.1 M HCl or 0.1 M NaOH. Subsequently, 1 g of the nanocomposite material was added to each flask. The flasks were sealed and agitated continuously for 24 hours to reach equilibrium. After equilibration, the suspensions were filtered, and the final pH (pH_f) of each filtrate was measured. The pH difference ($\Delta pH = pH_i - pH_f$) was plotted against the initial pH value (pH_i). The pH_{PZC} was identified as the pH at which $\Delta pH = 0$, corresponding to the point where the curve intersects the x-axis. This parameter provides critical insights into the surface charge behavior of the nanocomposites, influencing their adsorption performance in aqueous environments.

4) Adsorption experiments

The ammonium adsorption performance of the $MnFe_2O_4$/biochar nanocomposites (MFO@CFB and MFO@CFA) was evaluated under various experimental conditions: solution pH (3–8), contact time (5–120 min), adsorbent dosage (0.2–3 g L^{-1}) and initial ammonium concentration (10–60 mg L^{-1}). The initial ammonium concentration was standardized at 20 g L^{-1} for the baseline experiments. Adsorption studies were conducted in 250 mL beakers with continuous agitation at 120 rpm using an IKA horizontal shaker maintained at ambient temperature (25 ± 2 °C). Postadsorption, the suspensions were allowed to settle and filter, and the residual ammonium concentration in the filtrate was quantified via a UV–Vis spectrophotometer (Model 730, Japan) at a wavelength of 450 nm. A standard calibration curve ($y = 0.1053x - 0.0004$, $R^2 = 0.9991$) was employed for accurate concentration determination. All experiments were performed in triplicate, and the mean values were used for subsequent analysis.

The adsorption capacity (q_e, mg g^{-1}) and removal efficiency (H, %) were calculated via Eqs. 1 and 2:

$$q_e = (C_0 - C_e)V/m \quad \text{(Eq.1)}$$

$$H = C_0 - C_e/C_0 \times 100\% \quad \text{(Eq.2)}$$

where q_e is the adsorption capacity of the material (mg g^{-1}); C_o is the initial ammonium concentration (mg. L^{-1}); C_e: equilibrium ammonium concentration (mg L^{-1}); V: volume of solution (L); m: mass of material (g).

Data processing was performed via Microsoft Excel, whereas adsorption isotherms and kinetic modeling were analyzed via Origin 2025b software.

Adsorption kinetic and isotherm models:

The NH_4^+ adsorption capacity of MFO@CFB or MFO@CFA at a specific time t (q_t, mg g^{-1}) and at equilibrium (q_e, mg g^{-1}) was determined via Eqs. 3 and 4:

$$q_e = (C_0 - C_e)V/W \quad \text{(Eq.3)}$$

$$q_r = (C_0 - C_t)V/W \quad \text{(Eq.4)}$$

In these equations, C_0, C_t and C_e (mg L^{-1}) denote the concentrations of NH_4^+, the concentration at time t, and the equilibrium concentration, respectively. V (L) represents the volume of the NH_4^+ solution utilized, and W (g) corresponds to the dry weight of the MFO@CFB or MFO@CFA adsorbent.

The adsorption kinetics of NH_4^+ onto MFO@CFB or MFO@CFA were analyzed via two well-recognized models: the pseudo-first-order model and the pseudo-second-order model. The mathematical formulations of these models are detailed as shown in Eqs. 5 and 6:

Pseudo-first-order model:

$$\ln(q_e - q_t) = \ln q_e - k_1 t \quad \text{(Eq.5)}$$

Pseudo-second-order model:

$$t/q_t = (1/k_2 q_e^2) + (1/q_e)t \quad \text{(Eq.6)}$$

where q_e and q_t (mg g^{-1}) represent the adsorption capacities at equilibrium and at a specific time t (min), respectively; k_1 (min^{-1}) and k_2 (g mg^{-1} min^{-1}) are the rate constants of the pseudo-first-order and pseudo-second-order models, respectively.

The Langmuir and Freundlich models were employed to characterize the adsorption isotherms of NH_4^+ onto MFO@CFB or MFO@CFA. The Langmuir model assumes that adsorption occurs on a homogenous monolayer surface, where all adsorption sites possess equal energy and are energetically identical. In contrast, the Freundlich model describes adsorption on a heterogeneous surface, where the active sites exhibit varying energy levels, reflecting a more complex interaction. The mathematical expressions for these models are shown in Eqs. 7 and 8:

Langmuir model:

$$q_e = (q_m K_L C_e)/(1 + K_L C_e) \quad \text{(Eq.7)}$$

Freundlich model:

$$q_e = K_F C_e^{1/n} \quad \text{(Eq.8)}$$

where q_e (mg g^{-1}) is the adsorption capacity at equilibrium, and q_m (mg g^{-1}) is the maximum adsorption capacity; C_e (mg L^{-1}) represents the equilibrium con-

centration of NH_4^+ in the solution; K_L (L mg^{-1}) is the Langmuir constant, indicative of the adsorption energy; and K_F (mg g^{-1}) and n are the Freundlich constants, with n reflecting the adsorption intensity.

5) Material regeneration procedure

After the adsorption process, the spent adsorbent was recovered via an external magnetic field. The NH_4^+-saturated material was then immersed in a 0.1 M NaOH solution and magnetically stirred for 90 min. Subsequently, the material was thoroughly washed with deionized water until a neutral pH (~7) was reached, followed by drying at 80 °C for 12 h. The regenerated adsorbent was then reused for the subsequent adsorption cycle.

Results and discussion

1) Morphological characterization

The morphological characteristics of the synthesized materials were investigated by scanning electron microscopy (SEM, Hitachi S-4800), and representative images are presented in Figure 1. The pristine biochar derived from coffee husks exhibited a fibrous architecture characterized by elongated, densely packed fibers with a relatively smooth surface and minimal porosity (Figure 1a). This structure is typical of lignocellulosic biomass, indicating its inherent cellular structure (Puari et al., 2024; Zaitun et al., 2022). Such fibrous networks often exhibit smooth surfaces with minimal porosity, which can limit their adsorption capabilities (Adeniyi et al., 2020; Zhang et al., 2019). Following chemical activation with 0.3 M NaOH, the CFB biochar displays a significantly refined surface morphology characterized by a smoother texture, reduced fiber dimensions, and the formation of numerous surface voids and micropores (Figure 1b). The NaOH treatment likely enhances surface etching and removes residual organic impurities, increasing the surface area and porosity of the biochar (Puari et al., 2024). Further modification with 3 M HNO_3 results in CFA biochar, which has a highly porous structure with well-distributed micropores and mesopores, accompanied by a smoother surface texture (Figure 1c). The HNO_3 activation process introduces oxygen-containing functional groups (Melo et al., 2022) and enhances pore development through oxidative etching, significantly altering the surface morphology and improving the material's adsorption potential.

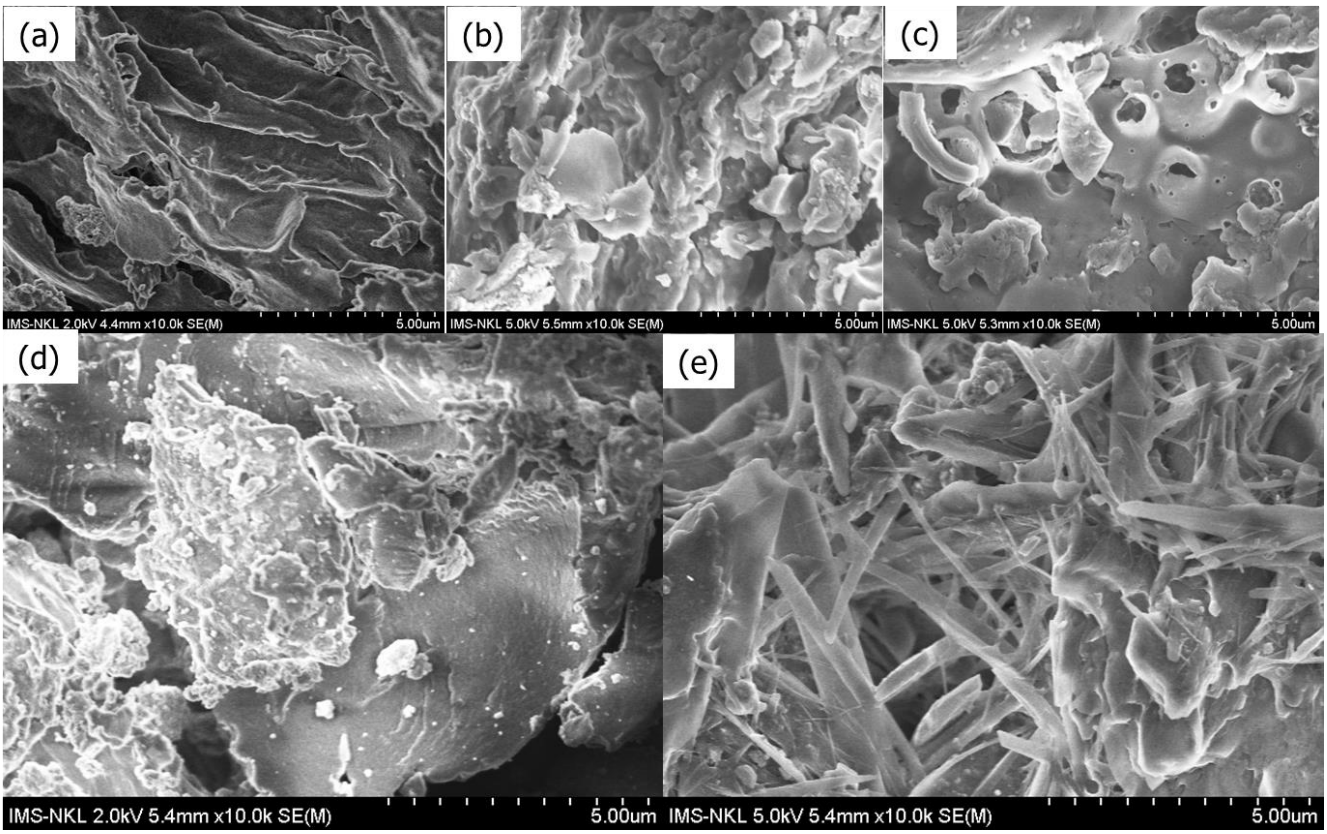

Figure 1 SEM images of (a) biochar, (b) CFB, (c) CFA, (d) MFO@CFB and (e) MFO@CFA.

SEM analysis of the $MnFe_2O_4$/biochar nanocomposites revealed distinct morphological transformations compared with those of the pristine and activated biochars, underscoring the successful integration of $MnFe_2O_4$ nanoparticles with the biochar matrix. The MFO@CFB composite (Figure 1d) exhibited a fine-grained structure with $MnFe_2O_4$ nanoparticles uniformly dispersed across the NaOH-activated biochar surface. These nanoparticles, ranging in size from 20–50 nm, appear as discrete entities or small aggregates, indicating effective anchoring of $MnFe_2O_4$ onto the biochar framework during the coprecipitation and hydrothermal syn-

thesis processes (Nigay et al., 2018). The enhanced magnetic properties of this composite, along with additional active sites for adsorption, suggest improved functionality over unmodified biochar (Hemlata, 2025). In contrast, the MFO@CFA composite (Figure 1e) displays a highly porous surface dominated by rod-like structures interspersed with multiple pores, where individual $MnFe_2O_4$ nanoparticles are less distinctly discernible. This morphology suggests a more integrated composite structure, potentially resulting from stronger chemical interactions between the HNO_3-activated biochar's oxygen-rich functional groups and the $MnFe_2O_4$ nanoparticles during hydrothermal treatment (Wang et al., 2022). The rod-like structures may arise from the restructuring of the biochar surface under acidic conditions, facilitating the formation of a more compact and porous hybrid material.

The observed morphological variations have profound implications for the adsorption performance of the nanocomposites. CFA biochar, characterized by greater porosity and surface area, in conjunction with the magnetic and catalytic attributes of $MnFe_2O_4$ in the MFO @CFA composite, increases ammonium ion accessibility and binding efficiency more than the MFO@CFB composite does (Jahani et al., 2023). The structural characteristics of MFO@CFA, particularly the rod-like formations, suggest a greater degree of surface functionalization, which may facilitate electrostatic interactions and ion exchange with NH_4^+ ions (Puari et al., 2024; Zhang et al., 2019). Moreover, the well-dispersed $MnFe_2O_4$ nanoparticles in MFO@CFB could favor rapid adsorption kinetics due to the numerous available discrete adsorption sites (Adeniyi et al., 2020). These findings underscore the efficacy of hybrid nanocomposites that integrate the porous carbon framework of coffee husk-derived biochar with the functional attributes of $MnFe_2O_4$ nanoparticles, offering tailored solutions for ammonium removal in wastewater management (Rasat et al., 2024).

The textural characteristics of the nanocomposites were further evaluated via N_2 adsorption–desorption analysis, with the BET surface area, total pore volume, and average pore size summarized in Table 1. The MFO@CFA nanocomposite resulted in a slightly greater BET surface area of 19.35 $m^2\ g^{-1}$ than the 18.38 $m^2\ g^{-1}$ for MFO@CFB. Similarly, compared with MFO@CFB, MFO@CFA presented a greater total pore volume (0.032 $cm^3\ g^{-1}$) and larger average pore diameter (6.21 nm) (0.027 $cm^3\ g^{-1}$ and 5.82 nm, respectively). These differences, although modest, are consistent with the enhanced pore development induced by HNO_3 activation, which promotes oxidative etching and structural expansion within the biochar matrix. The greater surface area and porosity of MFO@CFA contribute to improved accessibility of adsorption sites, particularly for NH_4^+ ions, and support the superior adsorption capacity of MFO@CFA observed in isotherm studies. In contrast, the lower surface area of MFO@CFB may limit the mass transfer efficiency despite the presence of well-dispersed $MnFe_2O_4$ nanoparticles, reinforcing the dominant role of surface functionalization over textural properties in determining the overall adsorption performance.

Fourier transform infrared spectroscopy (FTIR, Model 6300, Japan) was employed to elucidate the surface functional groups of the pristine biochar and $MnFe_2O_4$/biochar nanocomposites (MFO@CFB and MFO@CFA), and the resulting spectra are presented in Figure 2. The pristine biochar derived from coffee husks exhibited characteristic absorption bands at 3,452 cm^{-1}, corresponding to O–H stretching vibrations of hydroxyl groups; 1,635 cm^{-1}, attributed to C=C stretching in aromatic structures; and 1,384 cm^{-1}, indicative of C–O stretching in ethers or alcohols (Altaf et al., 2020; Yang et al., 2022). These bands reflect the oxygen-containing functional groups formed during the high-temperature pyrolysis of lignocellulosic coffee husk biomass, which contributes to its adsorption potential.

For the MFO@CFB and MFO@CFA nanocomposites, similar functional groups (O–H, C=C, and C–O) are observed but with slight shifts in wavenumber compared with those of the pristine biochar. These shifts suggest interactions between the biochar surface functional groups and the $MnFe_2O_4$ nanoparticles, likely due to coordination or hydrogen bonding. A distinctive absorption band at 586 cm^{-1}, corresponding to Mn–Fe–O stretching vibrations (Nguyen et al., 2021), is observed in both the MFO@CFB and MFO@CFA spectra, confirming the successful incorporation of $MnFe_2O_4$ nanoparticles into the biochar matrix and the formation of a hybrid nanocomposite structure. Notably, the MFO @CFA composite exhibited a unique COO^- stretching band at 2,364 cm^{-1}, which was absent in MFO@CFB and pristine biochar. This band is attributed to carboxylate groups formed during HNO_3 treatment, which introduce oxygen-rich functionalities through oxidative processes. The C–O stretching band at 1,384 cm^{-1} becomes significantly more intense, suggesting an increased concentration of carboxylic acid (–COOH) and carboxylate ($–COO^-$) groups. The transformation of carboxylic groups into carboxylate species likely results from deprotonation under acidic or subsequent alkaline conditions during synthesis. The higher density of negatively charged $–COO^-$ groups in MFO@CFA enhances electrostatic interactions with cationic species, such as NH_4^+, thereby improving its adsorption capacity in aqueous environments (Vu et al., 2017). The distinct surface chemistry of MFO@CFA, characterized by a greater abundance of oxygen-containing functional groups, makes it a superior adsorbent than MFO@CFB for cationic pollutants.

The differences in the FTIR spectra between MFO@CFB and MFO@CFA highlight the impact of

activation methods on surface functionalization. The NaOH activation in MFO@CFB enhances the number of hydroxyl groups, promoting hydrogen-bonding interactions, whereas the HNO_3 treatment in MFO@CFA introduces acidic functionalities that favor electrostatic and ion-exchange mechanisms. These tailored surface chemistries, combined with the catalytic and magnetic properties of $MnFe_2O_4$, underscore the versatility of the nanocomposites for ammonium removal.

Table 1 BET surface area, pore volume, and average pore size of the $MnFe_2O_4$/biochar nanocomposites

Material	BET surface area (m^2 g^{-1})	Pore volume (cm^3 g^{-1})	Pore size (nm)
MFO@CFB	18.38	0.027	5.82
MFO@CFA	19.35	0.032	6.21

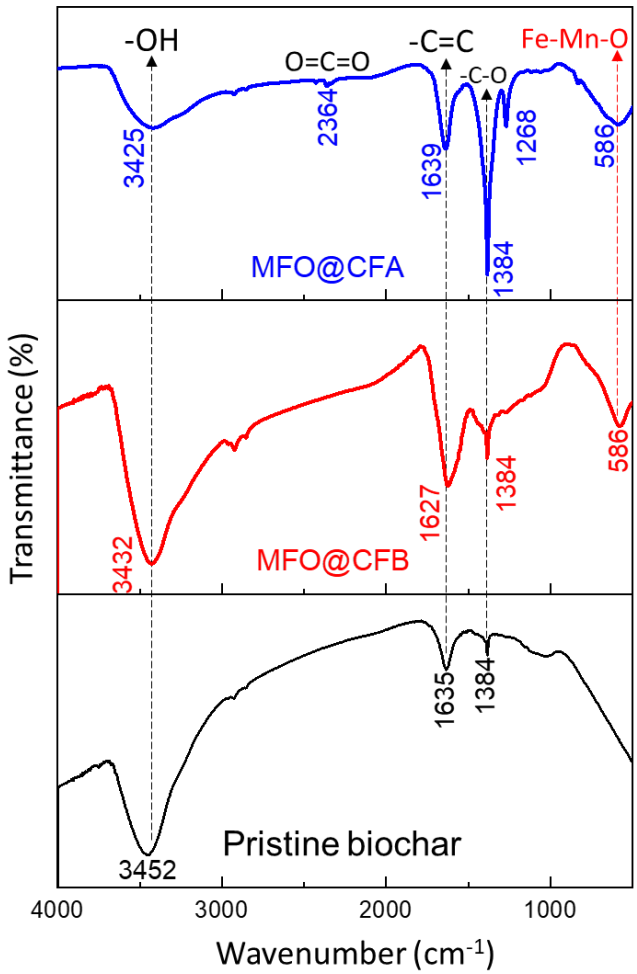

Figure 2 FTIR spectra of pristine biochar, MFO@CFB and MFO@CFA.

The point of zero charge (pH_{PZC}), defined as the pH at which the net surface charge of a material is zero, is a critical parameter governing adsorption behavior in aqueous systems. At pH values above the pH_{PZC}, the material's surface becomes negatively charged, facilitating electrostatic attraction with cationic species such as NH_4^+. Conversely, at pH values below the pH_{PZC}, the surface acquires a positive charge, favoring the adsorption of anionic species (Ciğeroğlu an Yıldırır, 2020). The pH_{PZC} of the MFO@CFB and MFO@CFA nanocomposites was determined via a pH titration method, and the results are presented in Figure 3a. The pH_{PZC} values for MFO@CFB and MFO@CFA were 5.0 and 3.15, respectively. The lower pH_{PZC} of MFO@CFA is attributed to the greater abundance of carboxyl (–COOH) and carboxylate ($–COO^-$) groups introduced by HNO_3 activation, which imparts a more acidic surface character. In contrast, NaOH-activated MFO@CFB has a higher pH_{PZC}, reflecting a relatively less acidic surface due to the predominance of hydroxyl and aliphatic groups. These low pH_{PZC} values indicate that both nanocomposites are predominantly negatively charged under typical environmental pH conditions (pH > 5), promoting electrostatic interactions with cationic NH_4^+ ions. The lower pH_{PZC} of MFO@CFA suggests a broader pH range for effective ammonium adsorption, as its surface remains negatively charged even under slightly acidic conditions, enhancing its applicability in diverse wastewater matrices.

The pH_{PZC} results provide a mechanistic basis for optimizing adsorption conditions. For example, operating at pH values above 3.15 for MFO@CFA and 5.0 for MFO@CFB maximizes electrostatic attraction, thereby improving ammonium removal efficiency. The differences in pH_{PZC} between the two composites align with their FTIR profiles, where the higher density of acidic functional groups in MFO@CFA correlates with its lower pH_{PZC} and enhanced cationic adsorption capacity. These findings underscore the role of surface charge in governing adsorption performance and highlight the tailored design of MFO@CFA for superior ammonium uptake. Additional studies, such as zeta potential measurements across a range of pH values, could further elucidate the surface charge dynamics and their impact on adsorption kinetics and isotherms, providing a comprehensive understanding of nanocomposite behavior in aqueous environments.

2) Factors influencing the ammonium adsorption capacity of composite materials

2.1) Effect of pH on ammonium adsorption capacity

The influence of the solution pH on the ammonium adsorption capacity (q) of the $MnFe_2O_4$/biochar nanocomposites (MFO@CFA and MFO@CFB) was systematically evaluated across a pH range of 3–8, and the results are shown in Figure 3b. For the MFO@CFA composite, the adsorption capacity markedly increased from 3.11 mg g^{-1} at pH 4 to a maximum of 16.33 mg g^{-1} at pH 6, corresponding to an increase in removal efficiency from 9.32% to 48.82%. Beyond pH 6, a gradual decline in q_e was observed. Conversely, the MFO@

CFB composite demonstrated relatively stable adsorption behavior, with q increasing modestly from 9.37 mg g^{-1} at pH 3 to a peak of 15.12 mg g^{-1} at pH 5, followed by a sharp decrease at higher pH values.

The pH-dependent adsorption performance is governed by the interplay of ammonium speciation and the surface charge properties of the nanocomposites, as determined by their point of zero charge (pH_{PZC}) (Figure 3a). Ammonium exists predominantly as a cationic NH_4^+ species at pH values below its pKa of approximately 9.25 (Ludewig et al., 2007), transitioning to neutral NH_3 under alkaline conditions (pH > 9). Consequently, optimal adsorption occurs in mildly acidic to neutral environments, where NH_4^+ is the dominant species and where electrostatic interactions with negatively charged nanocomposite surfaces are maximized (Elmoubarki et al., 2015). For MFO@CFA, at pH values above its pH_{PZC} of 3.15 (e.g., pH 4–6), the surface becomes increasingly negatively charged due to the deprotonation of oxygen-containing functional groups, such as carboxylic (–COOH) and carboxylate ($–COO^-$) groups, as evidenced by FTIR analysis (Figure 2). This negative surface charge enhances electrostatic attraction with NH_4^+ ions, resulting in a peak adsorption capacity at pH 6, where the balance between surface charge and NH_4^+ availability is optimized.

In contrast, for MFO@CFB, at pH values below its pH_{PZC} of 5.0, the surface is positively charged due to protonation of functional groups (e.g., $–COOH_2^+$), leading to electrostatic repulsion with NH_4^+ and H^+ ions, which decreases the adsorption efficiency. Under these conditions, ion exchange emerges as the dominant mechanism, where surface-bound N^+ or Na^+ ions, derived from –COOH or –COONa groups, are exchanged with NH_4^+, as described by the reactions shown in Eqs. 9 and 10:

$$R–COOH + NH_4^+ \rightarrow R–COONH_4^+ + H^+ \quad \text{(Eq.9)}$$

$$R–COONa + NH_4^+ \rightarrow R–COONH_4^+ + Na^+ \quad \text{(Eq.10)}$$

At pH values above 5.0, the MFO@CFB surface becomes negatively charged, promoting electrostatic interactions with NH_4^+. However, the modest increase in adsorption capacity suggests that ion exchange remains a significant contributor, with electrostatic attraction playing a secondary role. Under weakly alkaline conditions (pH > 7), both nanocomposites exhibit reduced adsorption performance due to two primary factors: (1) the conversion of NH_4^+ to neutral NH_3, which results in weaker interactions with the negatively charged surface due to diminished electrostatic and ion exchange mechanisms, and (2) competition from OH^- ions, which may neutralize or occupy active adsorption sites, further reducing NH_4^+ uptake.

The superior adsorption performance of MFO@CFA compared with that of MFO@CFB can be attributed to its lower pH_{PZC} (3.15) and higher density of oxygen-containing functional groups, particularly carboxylate ($–COO^-$) groups, as confirmed by the distinct COO^- stretching band at 2364 cm^{-1} in its FTIR spectrum (Figure 2). These groups enhance electrostatic interactions across a broader pH range, making MFO@CFA more effective in mildly acidic to neutral conditions. The optimal pH for ammonium adsorption was determined to be 6 for MFO@CFA and 5 for MFO@CFB, aligning with their respective pH_{PZC} values and the predominance of NH_4^+ in these ranges. These findings are consistent with previous studies on functionalized biochars, which reported enhanced cationic adsorption due to increased negative surface charge and oxygen-containing functional groups (Alshameri et al., 2018; Elmoubarki et al., 2015).

The pH-dependent adsorption behavior highlights the critical role of surface chemistry in optimizing ammonium removal. The lower pH_{PZC} of MFO@CFA provides a practical advantage for wastewater treatment applications, as it maintains a negatively charged surface even under slightly acidic conditions, broadening its operational pH range. This is particularly relevant for real-world wastewater matrices, which often exhibit variable pH levels.

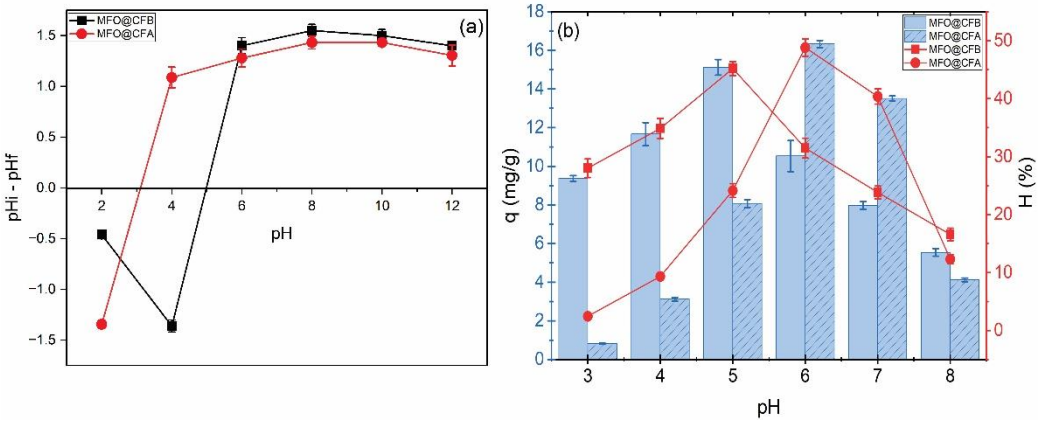

Figure 3 pH_{PZC} of composite materials (a) and effect of solution pH on the ammonium adsorption capacity of composite materials (b).

2.2) Effect of adsorption time on ammonium adsorption capacity

The effect of contact time on the ammonium adsorption capacity (q) of the $MnFe_2O_4$/biochar nanocomposites (MFO@CFB and MFO@CFA) was investigated over a time range of 5–120 min, and the results are presented in Figure 4a. Both nanocomposites exhibited a characteristic trend where q increased rapidly with contact time before reaching a plateau, indicative of adsorption equilibrium. Specifically, the MFO@CFB composite reached saturation at approximately 40 min, with a maximum adsorption capacity of 17.57 mg g^{-1}, whereas the MFO@CFA composite reached equilibrium more rapidly at 20 min, with a maximum q of 16.35 mg g^{-1}.

This temporal adsorption behavior aligns with classical adsorption kinetics, where the initial rapid uptake is driven by the availability of abundant active sites and a steep concentration gradient between the aqueous phase (containing NH_4^+ ions) and the adsorbent surface (El-Nabarawy et al., 1996). During the early stages of adsorption, the high density of unoccupied sites facilitates rapid ion transfer, resulting in a sharp increase in q. As the contact time progresses, the number of available active sites diminishes due to progressive occupation by NH_4^+ ions, weakening adsorptive interactions. Consequently, a dynamic equilibrium is established between the adsorption and desorption processes, leading to a slower, nearly linear increase in q_e until saturation is achieved (Long et al., 2008). The plateau observed in the adsorption curves reflects the point at which the rate of NH_4^+ uptake equals the rate of desorption, indicating the maximum adsorption capacity under the experimental conditions.

The faster equilibrium time for MFO@CFA (20 min) than for MFO@CFB (40 min) can be attributed to the distinct surface chemistry and morphology of the two composites. As revealed by FTIR analysis, MFO@CFA possesses a greater abundance of oxygen-containing functional groups, particularly carboxylate ($–COO^-$) groups, which enhance electrostatic attraction with cationic NH_4^+ ions. This strong electrostatic interaction likely accelerated the occupation of adsorption sites, enabling MFO@CFA to reach equilibrium more rapidly. Additionally, the porous, rod-like morphology of MFO@CFA may provide greater accessibility to active sites, further facilitating rapid ion transfer. In contrast, the MFO@CFB composite, with its fine-grained structure and dispersed $MnFe_2O_4$ nanoparticles, relies more heavily on ion exchange mechanisms involving –COOH and –COONa groups, which may exhibit slower kinetics because of the need for ion displacement. The lower density of acidic functional groups in MFO@CFB, as confirmed by its higher pH_{PZC} of 5.0 compared with 3.15 for MFO@CFA, further supports the observed slower equilibrium time.

These findings are consistent with previous studies on functionalized biochars and metal oxide composites, which reported that the presence of oxygen-rich functional groups and porous structures enhances the adsorption kinetics for cationic species (Asghar et al., 2020; Taguba et al., 2021). The faster saturation of MFO@CFA suggests its potential for applications requiring rapid pollutant removal, such as in continuous-flow wastewater treatment systems. Conversely, the slightly higher maximum q of MFO@CFB (17.57 mg g^{-1} vs. 16.35 mg g^{-1} for MFO@CFA) indicates a greater total capacity, possibly due to the contribution of $MnFe_2O_4$ nanoparticles, which provide additional adsorption sites through surface complexation or coordination with NH_4^+ ions. The interplay between kinetics and capacity highlights the tailored design of these nanocomposites: MFO@CFA excels in rapid adsorption, whereas MFO@CFB offers a marginally higher capacity at the cost of longer contact times. On the basis of these results, the optimal contact times for ammonium adsorption were 20 min for MFO@CFA and 40 min for MFO@CFB.

2.3) Effect of adsorbent content on the adsorption efficiency of ammonium

The effect of adsorbent dosage on the ammonium adsorption efficiency (H%) of the $MnFe_2O_4$/biochar nanocomposites (MFO@CFB and MFO@CFA) was investigated over a dosage range of 0.2 to 3 g L^{-1}, and the results are presented in Figure 4b. The adsorption efficiency increased with increasing adsorbent dosage, which was attributed to the greater availability of active adsorption sites, facilitating enhanced interactions with NH_4^+ ions. However, beyond a certain threshold, further increases in adsorbent dosage yielded diminishing returns, as the adsorption efficiency reached a plateau due to the saturation of available NH_4^+ ions in the solution relative to the excess number of adsorption sites.

For the MFO@CFB composite, the ammonium adsorption efficiency peaked at 61.12% at an adsorbent dosage of 1 g L^{-1}. Beyond this point, in the dosage range of 1.5–3 g L^{-1}, the efficiency stabilized and fluctuated slightly between 59.46% and 60.32%. Similarly, the MFO@CFA composite exhibited a maximum adsorption efficiency of 50.86% at a dosage of 0.6 g L^{-1}, with stabilization in the range of 1 to 3 g L^{-1}, where the efficiency varied marginally from 49.45% to 50.78%. Despite the lower maximum efficiency of MFO@CFA compared to MFO@CFB, the former required a lower optimal dosage (0.6 g L^{-1} vs. 1 g L^{-1} for MFO@CFB), suggesting higher efficiency per unit mass of adsorbent. On the basis of these results, optimal adsorbent dosages of 1 g L^{-1} for MFO@CFB and 0.6 g L^{-1} for MFO@CFA were selected for subsequent experiments to balance efficiency and material economy.

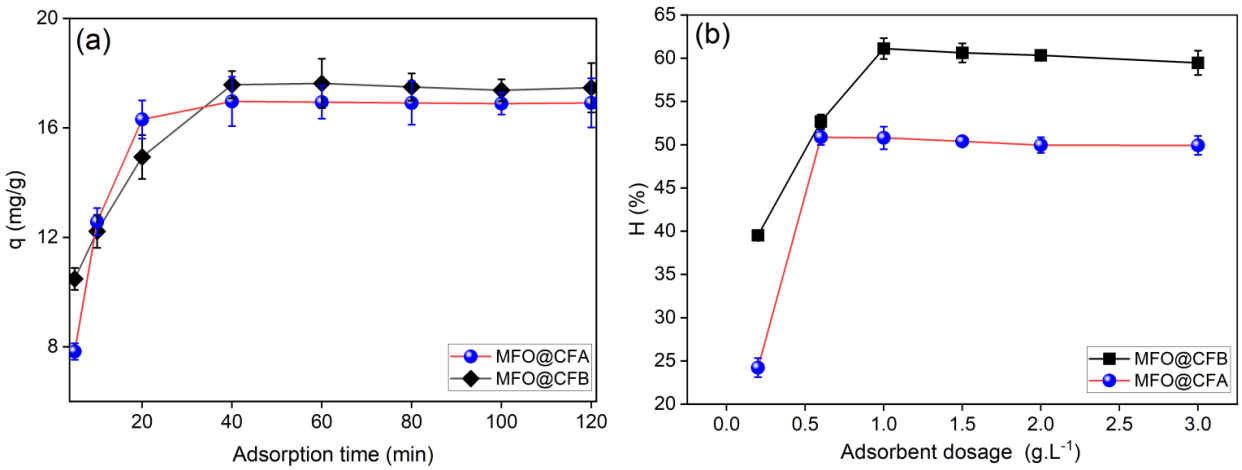

Figure 4 Effects of adsorption time (a) and adsorbent content (b) on the ammonium adsorption capacity of composite materials.

The observed trends are consistent with adsorption theory, where an increased adsorbent dosage enhances the number of available active sites, thereby improving NH_4^+ uptake until the solution's ammonium concentration becomes limiting (Do et al., 2022). The higher adsorption efficiency of MFO@CFB at its optimal dosage may be attributed to the contribution of $MnFe_2O_4$ nanoparticles, which provide additional adsorption sites through surface complexation or coordination, as evidenced by its fine-grained morphology with well-dispersed materials (Begum et al., 2020). The slightly greater maximum adsorption capacity of MFO@CFB (17.57 mg g^{-1}) than of MFO@CFA (16.35 mg g^{-1}) further supports its ability to accommodate more NH_4^+ ions at higher dosages. However, the lower optimal dosage of MFO@CFA highlights its superior efficiency per unit mass, likely due to its highly porous, rod-like structure and greater density of oxygen-containing functional groups.

The stabilization of the adsorption efficiency at higher dosages suggests the presence of excess adsorption sites relative to the available NH_4^+ ions, leading to underutilization of the adsorbent's capacity. This phenomenon may also result from particle aggregation at higher dosages, which reduces the effective surface area and hinders access to internal adsorption sites (Begum et al., 2020). The lower optimal dosage of MFO@CFA indicates a higher surface area-to-mass ratio and greater site accessibility, as supported by its porous morphology. The differences in the optimal dosage and efficiency between MFO@CFB and MFO@CFA reflect their distinct surface chemistries and morphologies. The NaOH-activated MFO@CFB, with a higher pH_{PZC}, relies on a combination of ion exchange and electrostatic interactions, requiring a higher dosage to achieve maximum efficiency. In contrast, HNO_3-activated MFO@CFA, with a lower pH_{PZC} and abundant $–COO^-$ groups, favors rapid electrostatic binding, achieving comparable efficiency at a lower dosage.

These findings have significant implications for the practical application of these adsorbents in wastewater treatment. The lower optimal dosage of MFO@CFA suggests potential cost savings and reduced material requirements, making it more suitable for large-scale applications where resource efficiency is critical. However, the higher maximum efficiency of MFO@CFB at 1 g L^{-1} may be advantageous in scenarios requiring maximum NH_4^+ removal, such as highly contaminated effluents.

2.4) Effect of initial concentration of ammonium on adsorption efficiency

The impact of the initial ammonium concentration on the adsorption capacity (q) of the $MnFe_2O_4$/biochar nanocomposites (MFO@CFB and MFO@CFA) was evaluated across a concentration range of 10 to 60 mg L^{-1}, and the results are depicted in Figure 5. The adsorption capacity increased progressively with increasing initial ammonium concentration for both composites. Specifically, for MFO@CFB, q increased from 10.5 mg g^{-1} at 10 mg L^{-1} to 25.0 mg g^{-1} at 60 mg L^{-1}, whereas for MFO@CFA, q increased from 11.0 mg g^{-1} at 10 mg L^{-1} to 33.5 mg g^{-1} at 60 mg L^{-1}. This trend reflects the enhanced driving force provided by the concentration gradient, which promotes the mass transfer of NH_4^+ ions from the aqueous phase to the adsorbent surface (Kim et al., 2021).

At lower initial concentrations (e.g., 10–20 mg L^{-1}), the abundance of unoccupied active sites on the nanocomposite surfaces ensures high adsorption efficiency, as the number of NH_4^+ ions is insufficient to saturate the available sites. As the initial concentration increases (e.g., 30–60 mg L^{-1}), the active sites become progressively occupied, leading to a gradual reduction in the proportion of adsorbed NH_4^+ relative to the total available ions, thus decreasing the adsorption efficiency. At higher concentrations (e.g., 50–60 mg L^{-1}), the adsorption capacity plateaus, indicating saturation of the adsorbent surfaces, beyond which additional

NH_4^+ ions remain in the solution due to the exhaustion of binding sites. This saturation behavior is consistent with the Langmuir isotherm model, where the maximum adsorption capacity is reached when all the active sites are occupied (Gao et al., 2015).

Among the investigated parameters, pH, contact time, adsorbent dosage, and initial concentration, the MFO@CFA composite consistently outperformed MFO @CFB in terms of adsorption capacity across the tested concentration range. For example, at 60 mg L^{-1}, MFO@CFA achieved a q of 33.5 mg g^{-1} compared with 25.0 mg g^{-1} for MFO@CFB, representing a 34% greater capacity. This superior performance can be attributed to the greater density of oxygen-containing functional groups, particularly carboxylate ($–COO^–$) groups, on the MFO@CFA surface, as confirmed by FTIR analysis. These groups enhance electrostatic interactions with NH_4^+ ions, facilitated by the composite's lower pH_{PZC} of 3.15 and its porous, rod-like morphology, which provides greater site accessibility. In contrast, MFO@CFB, with a higher pH_{PZC} of 5.0 and a fine-grained structure with dispersed $MnFe_2O_4$ nanoparticles, relies more on ion exchange mechanisms and surface complexation, resulting in a lower maximum capacity.

Furthermore, achieving comparable removal efficiencies with MFO@CFB required a higher adsorbent dosage than with MFO@CFA. For example, to attain an efficiency of approximately 50%, MFO@CFA required only 0.6 g L^{-1}, whereas MFO@CFB necessitated 1 g L^{-1}. This discrepancy underscores the greater efficiency per unit mass of MFO@CFA, likely due to its optimized surface chemistry and structural properties (Chen et al., 2021). The higher capacity of MFO@CFA at elevated concentrations suggests its suitability for treating highly contaminated wastewater, where NH_4^+ levels may exceed 50 mg L^{-1}, a common scenario in agricultural or industrial effluents.

The concentration-dependent adsorption behavior has significant implications for practical applications. The rapid increase in q at lower concentrations indicates that both nanocomposites are effective for treating dilute ammonium solutions, such as domestic wastewater. However, the plateau at higher concentrations highlights the need for dosage optimization or multistage adsorption processes to handle concentrated effluents. The superior performance of MFO@CFA at higher concentrations makes it a promising candidate for industrial wastewater treatment, where cost-effective, high-capacity adsorbents are critical.

2.5) Adsorption kinetics studies

On the basis of the experimental data investigating the influence of adsorption time on the ammonium adsorption capacity of MFO@CFB and MFO@CFA, pseudo-first-order and pseudo-second-order models were applied. The corresponding kinetic parameters are summarized in Figure 6 and Table 2.

The experimental results indicate that the correlation coefficients (R^2) for the pseudo-first-order models of MFO@CFB and MFO@CFA are 0.7225 and 0.3261, respectively, and the correlation coefficients (R^2) for the pseudo-second-order models of MFO@CFB and MFO @CFA are 0.9975 and 0.9985, respectively. These values suggest that the ammonium adsorption kinetics of MFO@CFB and MFO@CFA are more accurately described by the pseudo-second-order kinetic model.

Furthermore, a comparison between the calculated equilibrium adsorption capacity (q_e) and the experimental value ($q_{e,exp}$) supports this conclusion. Specifically, the q_e value derived from the pseudo-second-order model of MFO@CFB (q_m = 17.83 mg g^{-1}) closely aligns with the experimental value ($q_{e,exp}$ = 17.37 mg g^{-1}), and the q_e value derived from the pseudo-second-order model of MFO@CFA (q_m = 17.51 mg g^{-1}) closely aligns with the experimental value ($q_{e,exp}$ = 16.97 mg g^{-1}).

This finding confirms that the ammonium adsorption process on MFO@CFB and MFO@CFA follows the pseudo-second-order kinetic model, where the adsorption rate at time t is proportional to the square of the adsorption capacity. Consequently, the adsorption rate decreases significantly as the system approaches equilibrium.

2.6) Adsorption isotherm analysis

The adsorption isotherms of ammonium onto the $MnFe_2O_4$/biochar nanocomposites (MFO@CFB and MFO@CFA) were evaluated via the linear forms of the Langmuir and Freundlich models, and the results are presented in Figure 7 and summarized in Table 3. The Langmuir isotherm, depicted in Figure 7a, assumes monolayer adsorption onto a homogeneous surface with a finite number of identical sites. The Freundlich isotherm, shown in Figure 7b, describes multilayer adsorption on a heterogeneous surface.

Adsorption isotherm analysis of the $MnFe_2O_4$/biochar nanocomposites revealed distinct behaviors when modeled via the Langmuir and Freundlich equations. For the Langmuir model, MFO@CFB has a maximum adsorption capacity (q_m) of 28.73 mg g^{-1} with an equilibrium constant (K_1) of 0.105 L mg^{-1} and R^2 = 0.9798, whereas MFO@CFA has a significantly higher q_m of 55.25 mg g^{-1}, a lower K_1 of 0.046 L mg^{-1}, and R^2 = 0.988. The high R^2 values (>0.97) support monolayer adsorption on relatively homogeneous surfaces for both materials (Begum et al., 2020). The elevated q_m of MFO @CFA is attributed to its greater density of oxygen-containing functional groups, particularly deprotonated carboxylate ($–COO^–$) sites, as confirmed by FTIR, which increases the total number of available binding sites.

The K_1 parameter reflects the apparent binding affinity of NH_4^+ in the studied concentration range (10–60 mg L^{-1}). The higher K_1 of MFO@CFB indicates a stronger average binding energy per adsorbed ion, likely due to ion exchange-dominated interactions with the –COOH and –COONa groups on its NaOH-activated surface. This suggests that MFO@CFB may retain NH_4^+ more tenaciously at low-to-moderate concentrations (<30 mg L^{-1}), where site occupancy is limited. In contrast, the lower K_1 of MFO@CFA reflects weaker individual binding but is compensated by its nearly double monolayer capacity, driven by widespread electrostatic attraction across a broader pH and concentration range.

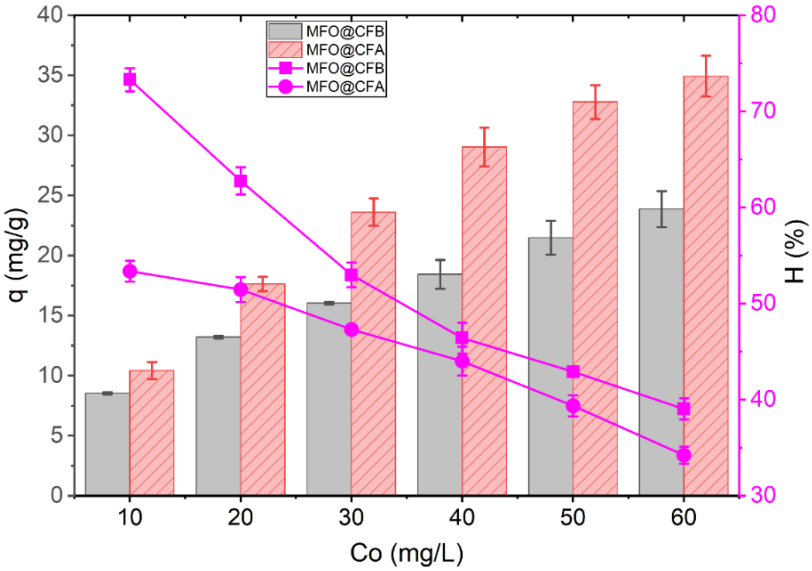

Figure 5 Effect of ammonium concentration on the ammonium adsorption capacity of composite materials.

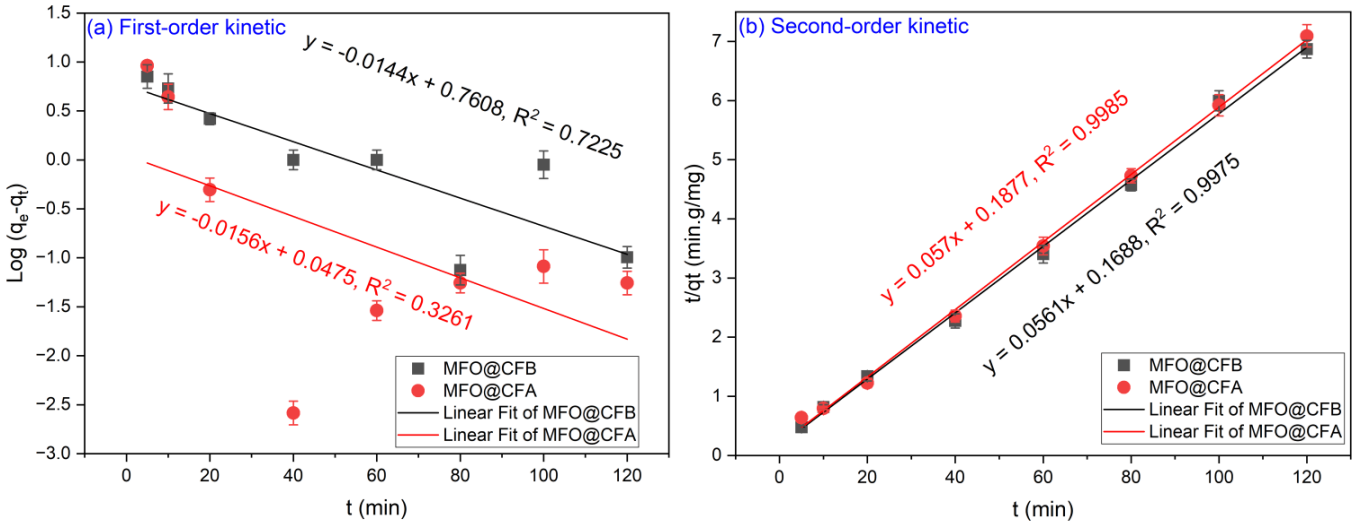

Figure 6 Linear first-order (a) and second-order (b) adsorption kinetics equations for ammonium adsorption on composite materials.

Table 2 Parameters of the kinetic models of ammonium adsorption using MFO@CFB and MFO@CFA

Composite materials	First-order kinetic model			Second-order kinetic model			$q_{e,exp}$ (mg g^{-1})
	$q_{m,cal}$ (mg g^{-1})	k_1 (min^{-1})	R^2	$q_{m,cal}$ (mg g^{-1})	k_2 (g mg^{-1} min^{-1})	R^2	
MFO@CFB	5.77	0.0332	0.7225	17.83	0.0186	0.9975	17.37
MFO@CFA	1.12	0.0359	0.3261	17.51	0.0177	0.9985	16.97

Table 3 Parameters of the adsorption isotherm models for ammonium adsorption onto composite materials

Composite materials	Langmuir model			Freundlich model		
	q_m (mg g^{-1})	K_L	R^2	K_F	1/n	R^2
MFO@CFB	28.73	0.105	0.9798	5.5	0.405	0.9955
MFO@CFA	55.25	0.046	0.988	4.075	0.609	0.9666

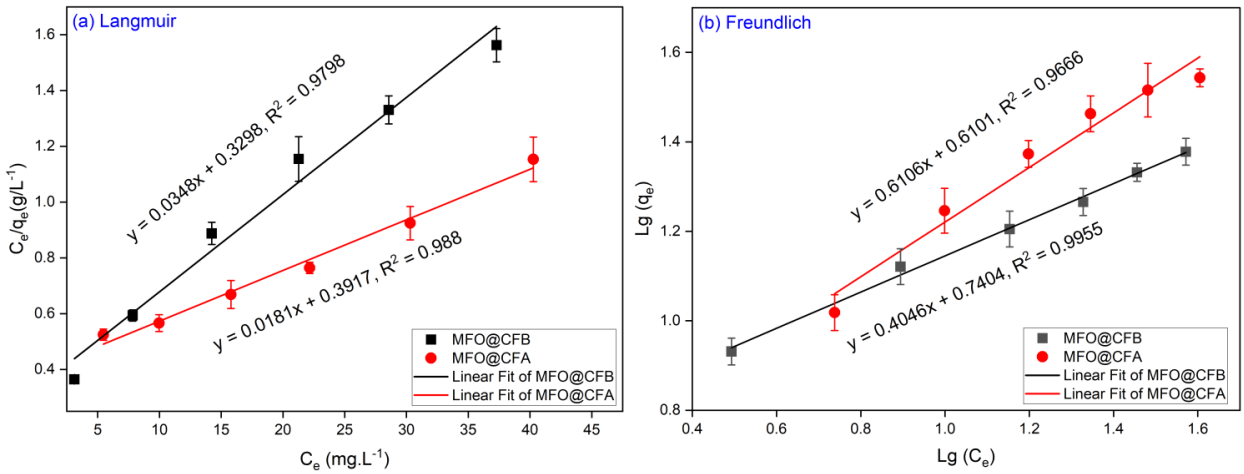

Figure 7 Linear Langmuir (a) and Freundlich (b) adsorption isotherms for ammonium adsorption by composite materials.

In the Freundlich model, MFO@CFB yields K_F = 5.5 mg g^{-1}(L mg^{-1})1/n, 1/n = 0.405, and R^2 = 0.9955, whereas MFO@CFA yields K_F = 4.075 mg g^{-1} (L mg^{-1})1/n, 1/n = 0.609, and R^2 = 0.9666. The superior R^2 for MFO@CFB indicates a better fit to the Freundlich model, reflecting a more heterogeneous surface with a wider distribution of binding energies, which is consistent with dispersed $MnFe_2O_4$ nanoparticles and NaOH-induced surface restructuring (Song et al., 2021). The 1/n values (<1 for both) confirm favorable adsorption; however, the lower 1/n of MFO@CFB signifies stronger adsorption at low surface coverage due to higher site uniformity, whereas the higher 1/n of MFO@CFA indicates greater energetic heterogeneity, enhancing uptake at high NH_4^+ loadings.

These contrasting adsorption behaviors have significant implications for the practical application of these nanocomposites in wastewater treatment. The superior q_m of MFO@CFA, in conjunction with its porous, rod-like morphology and a lower point of zero charge (pH_{PZC} of 3.15), enhances the accessibility and electrostatic attraction of NH_4^+ ions over a broader concentration range. These properties render MFO@CFA highly effective for treating effluents with elevated ammonium concentrations, such as those encountered in agricultural runoff or industrial discharges. Conversely, the higher K_L and more homogeneous adsorption site distribution observed for MFO@CFB imply that it may be more effective in systems with moderate ammonium levels, where strong binding affinity and consistent adsorption kinetics are essential for sustained treatment performance (Begum et al., 2020). The dual-model applicability of these nanocomposites underscores their complementary strengths, with MFO@CFA excelling in maximum adsorption capacity and MFO@CFB demonstrating robust site-specific affinity, thereby offering a versatile toolkit for engineered ammonium removal systems in dynamic wastewater environments.

2.7) Regeneration and reusability

Figure 8 shows the reusability of the composite materials for ammonium adsorption across five consecutive adsorption–desorption cycles. The adsorption capacity (q) of MFO@CFB gradually decreased from 28.73 mg g^{-1} in the initial cycle to 17.18 mg g^{-1} by the fifth cycle. In addition, the q of MFO@CFA also progressively decreased, from 55.25 mg g^{-1} in the initial cycle to 33.72 mg g^{-1} by the fifth cycle. This reduction can be attributed to several factors, including surface fouling resulting from residual ammonium ions or other impurities, structural degradation of the composite material during repeated cycles, and inefficiencies in the regeneration process, which may render some active sites less effective in subsequent cycles.

Despite the observed decrease in adsorption capacity, the MFO@CFB and MFO@CFA composites retain more than 50% of their initial capacity after five cycles, thereby indicating a favorable level of reusability. The efficient regeneration was attributed to alkaline desorption, which weakened the electrostatic interactions between the NH_4^+ ions and surface functional groups, whereas the $MnFe_2O_4$ phase remained stable, enabling rapid magnetic separation and minimizing material loss. This performance underscores the potential applicability of the MFO@CFB and MFO@CFA composites in practical wastewater treatment scenarios. However, to further increase their recyclability, improvements in material design or regeneration methodologies may be necessary to mitigate capacity loss over successive cycles.

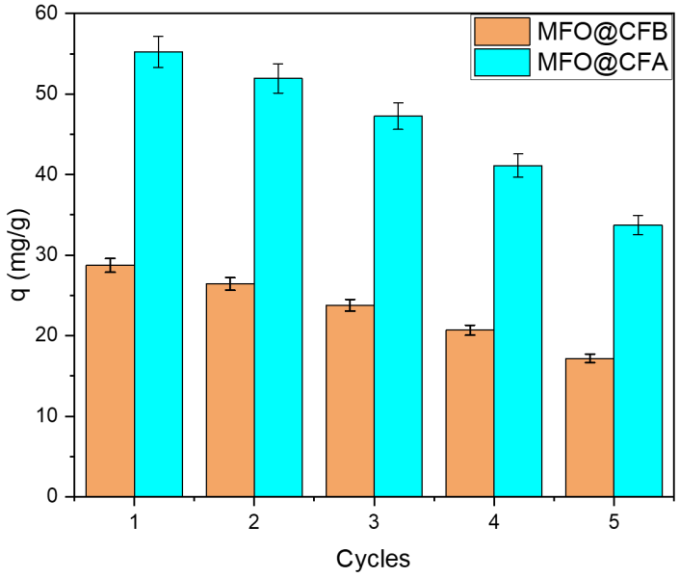

Figure 8 Recyclability of the composite materials for ammonium adsorption.

Conclusions

This study successfully developed two $MnFe_2O_4$-functionalized biochar nanocomposites from coffee husks, MFO@CFA (HNO_3-activated) and MFO@CFB (NaOH-activated), via coprecipitation and hydrothermal synthesis, demonstrating their efficacy in ammonium removal from aqueous solutions. Comprehensive characterization revealed that HNO_3 activation imparts MFO@CFA with a porous, rod-like morphology, greater BET surface area (19.35 m^2 g^{-1}), lower pH_{PZC} (3.15), and enriched carboxylate ($–COO^-$) functionality, collectively enabling a Langmuir maximum adsorption capacity of 55.25 mg g^{-1}—nearly double that of MFO@CFB (28.73 mg g^{-1})—along with faster equilibrium (20 min vs. 40 min) and a lower optimal dosage (0.6 g L^{-1} vs. 1.0 g L^{-1}). Adsorption followed pseudo-second-order kinetics and was best described by the Langmuir model, with MFO@CFB showing higher binding affinity (K_1 = 0.105 L mg^{-1}) due to ion exchange mechanisms, whereas MFO@CFA excelled in capacity and pH robustness via electrostatic interactions. These findings address a critical gap in $MnFe_2O_4$-doped biochar systems, namely, insufficient surface charge density, limited porosity, and narrow pH operability, by introducing a novel dual acid–alkali activation strategy that significantly enhances NH_4^+ uptake. The valorization of coffee husk further promotes a sustainable, circular approach to wastewater treatment. However, while superior performance has been achieved in single-solute systems, NH_4^+ selectivity in multication matrices remains unconfirmed, and competitive adsorption studies (e.g., with K^+, Ca^{2+}) are essential for validating real-world applicability, which is a key limitation and priority for future investigations. Although the NH_4^+ adsorption capacity decreased progressively with repeated reuse (likely due to fouling, structural degradation, and regeneration inefficiencies), both composites still exhibited favorable recyclability and practical promise for wastewater treatment, while further optimization of material design and/or regeneration protocols is needed to mitigate capacity loss.

Data availability statement

Information and data used in the study will be disclosed upon request.

Author ORCID

Thuy-Tien Do: 0000-0001-5619-2193
Huu-Tap Van: 0000-0002-9584-8383
Thi-Minh-Thu Nguyen: 0009-0008-3297-7349

Author contributions

Thuy-Tien Do: Conceptualization, Methodology, Software, Investigation, Data curation, Writing – Original draft, Writing – Review & editing, Project administration, Funding acquisition
Huu-Tap Van: Software, Validation, Investigation, Writing – Original draft, Writing – Review & editing, Supervision
Thi-Minh-Thu Nguyen: Methodology, Formal analysis, Resources, Data curation, Visualization

Conflicts of interest

The authors declare that there are no conflicts of interest in competing financial or personal relationships that could have appeared to influence the work reported in this work.

References

Adeniyi, A. G., Abdulkareem, S. A., Ighalo, J. O., Onifade, D. V., Adeoye, S. A., & Sampson, A. E. (2020). Morphological and thermal properties of polystyrene composite reinforced with biochar from elephant grass (*Pennisetum Purpureum*). *Journal of Thermoplastic Composition Materials*, *35*,1532–1547.

Alshameri, A., He, H., Zhu, J., Xi, Y., Zhu, R., Ma, L., &

Tao, Q. (2018). Adsorption of ammonium by different natural clay minerals: Characterization, kinetics and adsorption isotherms. *Applied Clay Science*, *159*, 83–93.

Asghar, K., Qasim, M., & Das, D. (2020). Preparation and characterization of mesoporous magnetic $MnFe_2O_4$@$mSiO_2$ nanocomposite for drug delivery application. *Materialstoday Proceedings*, *26*, 87–93.

Altaf, S., Ajaz, H., Imran, M. , Ul-Hamid, A., Naz, M., Aqeel, M., Shahzadi, A., Shahbaz, A. & Ikram, M. (2020). Synthesis and characterization of binary selenides of transition metals to investigate its photocatalytic, antimicrobial and anticancer efficacy. *Applied Nanoscience*, *10* 2113–2127.

Begum, S. A., Golam Hyder, A. H. M., Hicklen, Q., Crocker, T., & Oni, B. (2020). Adsorption characteristics of ammonium onto biochar from an aqueous solution. *AUQA – Water Infrastructure, Ecosystems and Society*, *70*(1), 113–122.

Chen, M., Wang, F., Zhang, D., Yi, W., & Liu, Y. (2021). Effects of acid modification on the structure and adsorption NH_4^+-N properties of biochar. *Renewable Energy*, *169*, 1343–1350.

Ciğeroğlu, Z., & Yıldırır, E. (2020). Vermicompost as a potential adsorbent for the adsorption of methylene blue dye from aqueous solutions. *Journal of the Turkish Chemical Society Section A: Chemistry*, *7*, 893–902.

Do, T. C. V., Pham, T. T. Y., & Pham, T. M. H. (2022). Ammonium removal by alkaline-activated coconut coir from synthetic and ground waters. *Asia-Pacific Journal of Chemical Enineering*,*18*, e2849.

El-Nabarawy, Th., Fagal, G. A., & Khalil, L. B. Removal of ammonia from aqueous solution using activated carbons. *Adsorption Science Technology*, *13*, 7–13.

Elmoubarki, R., Mahjoubi, F. Z., Tounsadi, H., Moustadraf, J., Abdennouri, M., Zouhri, A., El Albani, A., & Barka, N. (2015). Adsorption of textile dyes on raw and decanted Moroccan clays: Kinetics, equilibrium and thermodynamics. *Water Resources and Industry*, *9*, 16–29.

Gao, F., Xue, Y., Deng, P., Xiao-ru, C., & Yang, K. (2015). Removal of aqueous ammonium by biochars derived from agricultural residuals at different pyrolysis temperatures. *Chemical Speciation & Bioavailability*, *27*, 92–97.

Han, B., Butterly, C., Zhang, W., He, J., & Chen, D. (2021). Adsorbent materials for ammonium and ammonia removal: A review. *Journal of Cleaner Produc*tion, *283*, 124611.

Hemlata. (2025). Mechanical, thermal, morphological, and rheological behavior of recycled polypropylene/ pine needle biochar composite: An innovative approach towards circular economy. *Polymer Composites*, *46*, 8490–8507.

Huong, P.T. L, Tu, N., Lan, H., Thang, L. H., Van Quy, N., Tuan, P. A., Dinh, N. X., Phan, V.N. & Le, A.T. (2018). Functional manganese ferrite/graphene oxide nanocomposites: effects of graphene oxide on the adsorption mechanisms of organic MB dye and inorganic As(v) ions from aqueous solution. *RSC Advances*. *8*, 12376–12389.

Jahani, F., Maleki, B., Mansouri, M., Noorimotlagh, Z., & Mirzaee, S. A. (2023). Enhanced photocatalytic performance of Milkvetch-derived ciochar via ZnO–Ce nanoparticle decoration for reactive blue 19 dye removal. *Scientific Reports*, *13*, 17824.

Khalil, A., Sergeevich, N., & Borisova, V. N. (2018). Removal of ammonium from fish farms by biochar obtained from rice straw: Isotherm and kinetic studies for ammonium adsorption. *Adsorption Science & Technology*, *36*, 1294–1309.

Kim, G., Kim, Y. M., Kim, S., Cho, H., & Park, J. M. (2021). Magnetic steel slag biochar for ammonium nitrogen removal from aqueous solution. *Energies*, 14, 2682.

Kizito, S., Wu, S., Kirui, W. K., Lei, M., Lu, Q., Bah, H. & Dong, R. (2015). Evaluation of slow pyrolyzed wood and rice husks biochar for adsorption of ammonium nitrogen from piggery manure anaerobic digestate slurry. *Science of the Total Environment*, *505*, 102–112.

Liao, F., Diao, G., & Li, H. (2020). Green synthesis of graphene oxide-$MnFe_2O_4$ composites and their application in removing heavy metal ions. *Micro & Nano Letters*, *15*, 7–12.

Linh, N. H., Chi, N. K., Le Minh, T., Phuong, D. N., Tung, N. X., Tien, D. T., Minhyen, P. T. H., Linh, H., Chi, N. K., Le Minh, T., Phuong, D. N., Tung, N. X., Tien, D. T & Minh, P. T. H. (2024). Biochar of post-extraction coffee bean ground as materials for ammonium adsorption. *Vietnam Journal of Science and Technology*, *62*, 324–334.

Liu, Z., Xue, Y., Gao, F., Cheng, X., & Yang, K. (2016). Removal of ammonium from aqueous solutions using alkali-modified biochars. *Chemical Speciation & Bioavailability*, *28*, 26–32.

Long, X. L., Cheng, H., Xin, Z. L., Xiao, W. D., Li, W., Yuan, W. K. (2008). Adsorption of ammonia on activated carbon from aqueous solutions. *Environ-mental Progress*, *27*, 225–233.

Ludewig, U., Neuhäuser, B., & Dynowski, M. (2007). Molecular mechanisms of ammonium transport and accumulation in plants. *FEBS Letters*, *581*, 2301–2308.

Melo, A. L. F. C., Carneiro, M. T., Nascimento, A. M. S. S., Morais, A. Í. S., Bezerra, R. D. S., Viana, B. C., Osajima, J. A., & Silva-Filho, E. C. (2022). Biochar obtained from caryocar Brasiliense endocarp for removal of dyes from the aqueous medium. *Materials (Basel)*, *15*, 9076.

Nguyen, L. H., Nguyen, X. H., Nguyen, N. D. K., Van, H. T., Thai, V. N., Le, H. N., Pham, V. D., Nguyen,

N. A., Nguyen, T. P., & Nguyen, T. H. (2021). H_2O_2 modified-hydrochar derived from paper waste sludge for enriched surface functional groups and promoted adsorption to ammonium. *Journal of the Taiwan Institute of Chemical Engineers*, *126*, 119–133.

Nigay, P., Nzihou, A., White, C. E., & Soboyejo, W. O. (2018). Accumulators for the capture of heavy metals in thermal conversion systems. *Journal of Environmental Engineering*, *144*, 205.

Phuong, N. V., Hoang, N. K., Van Luan, L., & Tan, L. V. (2021). Evaluation of adsorption capacity in water of coffee husk-derived biochar at different pyrolysis temperatures. *International Journal of Agronomy*, *2021*, 1463814.

Puari, A. T., Rusnam, & Yanti, N. R. (2023). Removal of ammonium by biochar derived from exhausted coffee husk (ECH) at different carbonisation parameter. *IOP Conference Series: Earth and Environmental Sceince*, *1182*, 012037.

Puari, A. T. Rusnam, R. Yanti, N. R., Shukor, M. Y. (2024). Adsorption performance of biochar from exhausted coffee husk (ECH) under various carbonization parameters on copper (II) Ion in aqueous solution. *IOP Conference Series: Earth and Environmental Sceince*, 1426, 12011.

Rasat, M. S. M., Amin, M.F.M., Ahmad, M. I., Noor, A. M., Moktar, J., Yunus, A. A. M., Jemali, N. J. N., Majid, N. K. S. A., Amaludin, N. A., Bukhari, S. N. B., Darus, D. I. & Alamjuri, R. H. (2024). Bonding properties and morphological characteristics of torrefied pelletised biochar from palm oil industry's residues empty fruit bunch. *Bio Web of Conferences*, *131*, 5006.

Song, J., Srivastava, V., Kohout, T., Sillanpää, M., & Sainio, T. (2021). Montmorillonite-anchored magnetite nanocomposite for recovery of ammonium from stormwater and its reuse in adsorption of Sc^{3+}. *Nanotechnology for Environmental Engineering*, *6*, 1–14.

Taguba, M. A. M., Ong, D. C., Ensano, B. M. B., Kan, C. C., Grisdanurak, N., Yee, J. J., & de Luna, M. D. G. (2021). Nonlinear isotherm and kinetic modeling of Cu(II) and Pb(II) uptake from water by $MnFe_2O_4$/ chitosan nanoadsorbents. *Water*, *13*, 1662.

Tuyen, T. V., Chi, N. K., Tien, D. T., Tu, N., Quang, N. V., & Huong, P. T. L. Carbon-encapsulated $MnFe_2O_4$ nanoparticles: Effects of carbon on structure, magnetic properties and Cr(VI) removal efficiency. *Applied Physics A*, *126*, 577–589.

Vu, T. M., Trinh, V. T., Doan, D. P., Van, H. T., Nguyen, T. V., Vigneswaran, S., & Ngo, H. H. Removing ammonium from water using modified corncob-biochar. *Science of the Total Environment*, *579*, 612–619.

Vu, N. T. , & Do, K. U. (2023). Insights into adsorption of ammonium by biochar derived from low temperature pyrolysis of coffee husk. *Biomass Conversation and Biorefinery*, *13*, 2193–2205.

Wan, J., Deng, H., Shi, J., Zhou, L., & Su, T. (2014). Synthesized magnetic manganese ferrite nanoparticles on activated carbon for sulfamethoxazole removal. *CLEAN – Soil, Air, Water*, *42*, 1199–1207.

Wang, P., Stenrød, M., Wang, L., Yuan, S., Mao, L., Zhu, L., Zhang, L., Zhang, Y., Jiang, H., Zheng, Y., & Liu, X. (2022). Characterization of montmorillonite–biochar composite and its application in the removal of atrazine in aqueous solution and soil. *Frontiers in Environmental Science*, 10, 888252.

Yang, Y., Phuong Nguyen, T. M., Van, H. T., Nguyen, Q. T., Nguyen, T. H., Lien Nguyen, T. B., Hoang, L. P., Van Thanh, D., Nguyen, T. V., Nguyen, V. Q., Thang, P. Q., Yılmaz, M., & Le, V. G. (2022). ZnO nanoparticles loaded rice husk biochar as an effective adsorbent for removing reactive red 24 from aqueous solution. *Materials Science in Semiconductor Processing*, *150*, 106960.

Yang, H., Li, X., Wang, Y., Wang, J., Yang, L., Ma, Z., Luo, J., Cui, X., Yan, B., & Chen, G. (2023). Effective removal of ammonium from aqueous solution by ball-milled biochar modified with NaOH. *Processes*, *11*, 1671.

Zaitun, Z., Halim, A., Sa'dah, Y. & Cahyadi, R. (2022). Surface morphology properties of biochar Feedstock for soil amendment. *IOP Conference Series: Earth and Environmental Sceince*, *951*, 12034.

Zhang, L., Guo, J., Huang, X., Wang, W., Sun, P., Li, Y., Han, J. (2019). Functionalized biochar-supported magnetic $MnFe_2O_4$ nanocomposite for the removal of Pb(II) and Cd(II). *RSC Advances*, *9*, 365–376.